

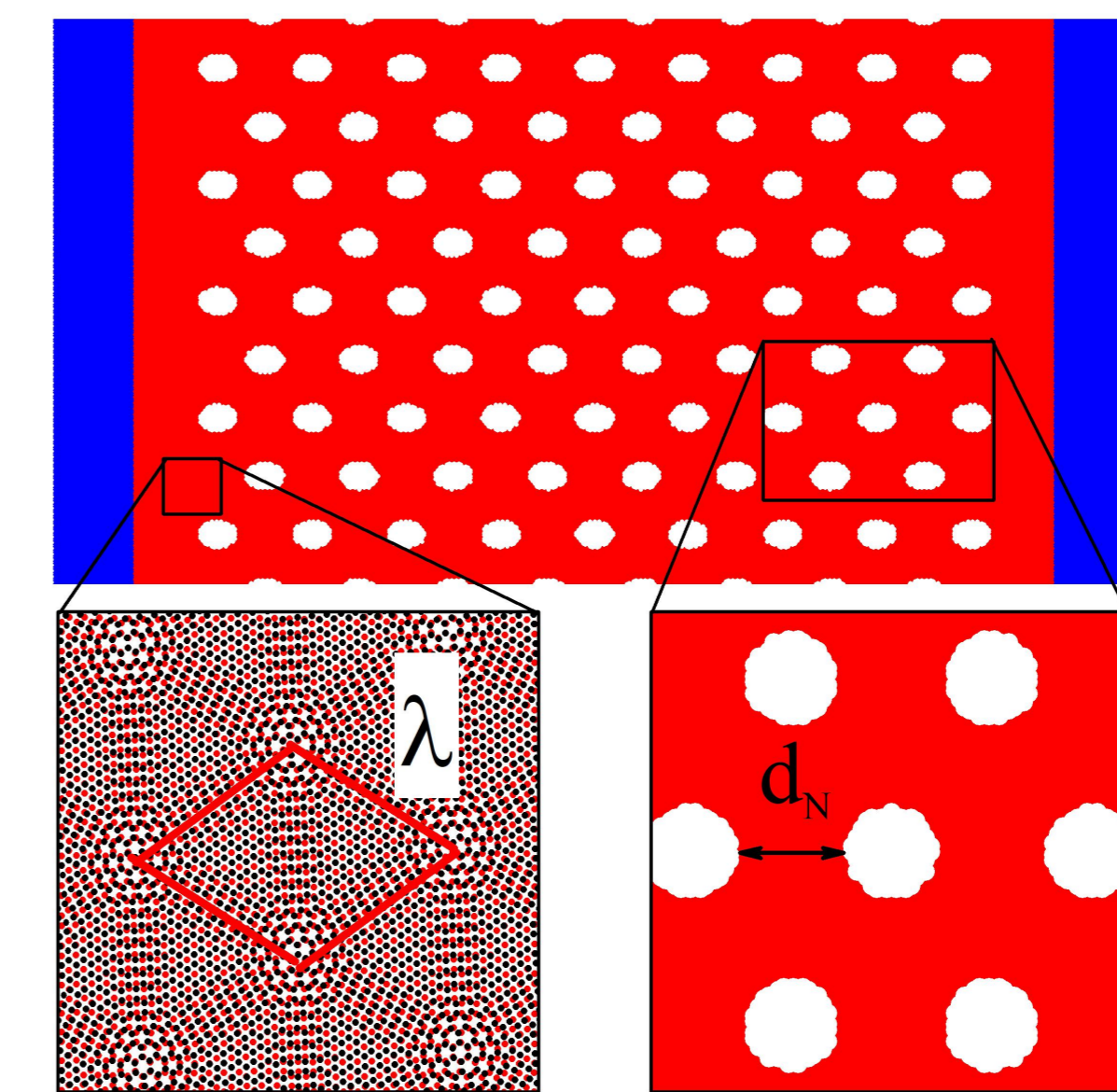
## Electronic structure and transport of antidot lattices in twisted heterostructures of graphene and hexagonal boron nitride

Yongping Du, Ning Xu, Xianqing Lin, and Antti-Pekka Jauho  
Center for Nanostructured Graphene, DTU Physics, Technical University of Denmark, Kongens Lyngby, Denmark

### Abstract

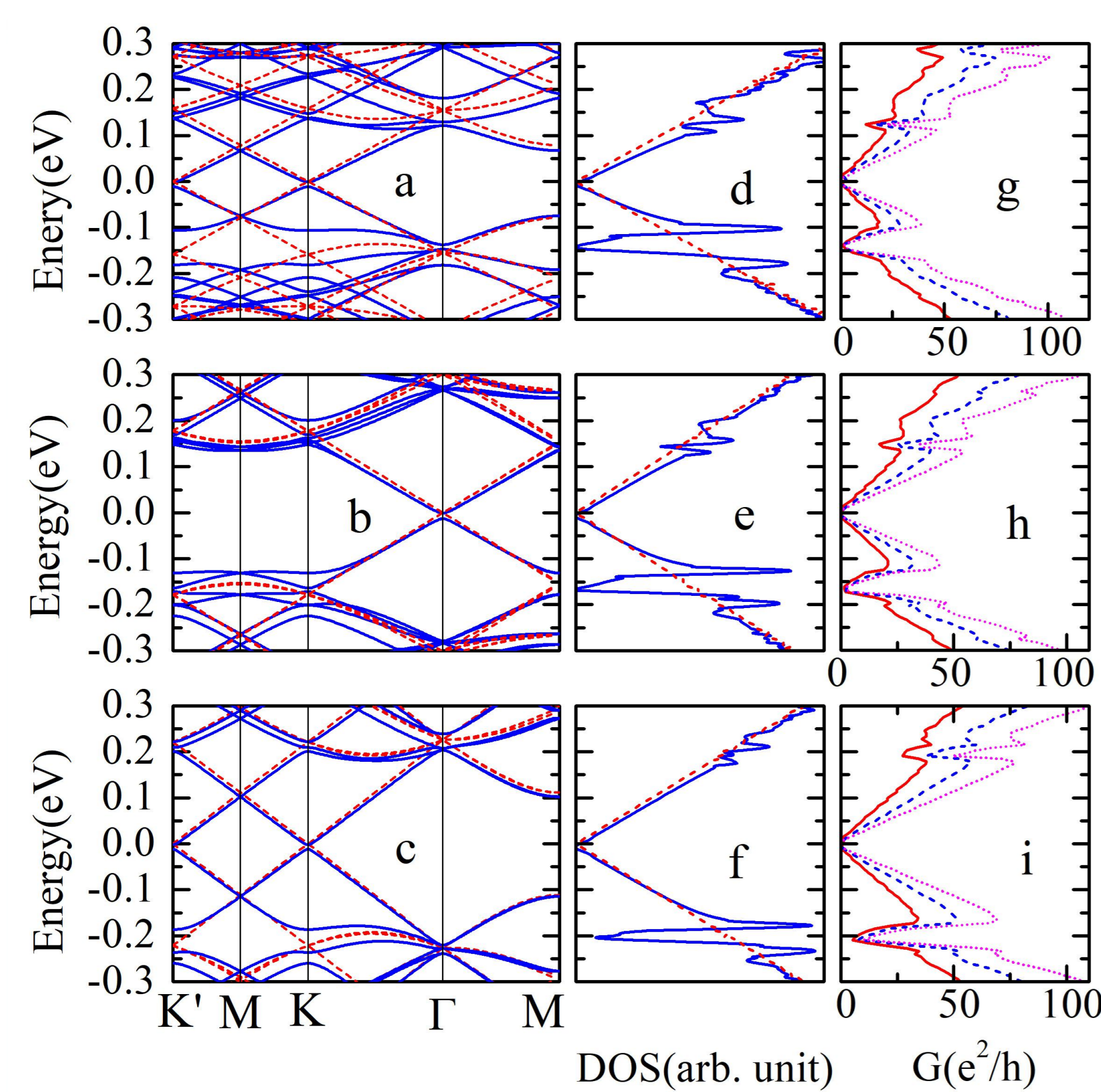
Encapsulating graphene in hexagonal Boron Nitride has several advantages: the highest mobilities reported to date are achieved in this way<sup>1</sup>, and precise nanostructuring of graphene becomes feasible through the protective hBN layers<sup>2</sup>. Nevertheless, subtle effects may arise due to the differing lattice constants of graphene and hBN, and due to the twist angle between the graphene and hBN lattices<sup>2,3,4</sup>. Here, we use a recently developed model which allows us to perform band structure and magnetotransport calculations of such structures, and show that with a proper account of the moiré physics an excellent agreement with experiments can be achieved, even for complicated structures such as disordered graphene, or antidot lattices on a monolayer hBN with a relative twist angle. Calculations of this kind are essential to a quantitative modelling of twistronic devices.

### Schematic of device



Schematic of the device. Blue areas are the left and right leads. The center with antidot lattice is the scattering area. The enlarged pictures show the moiré wave length  $\lambda$  and the neck width  $d_N$ .

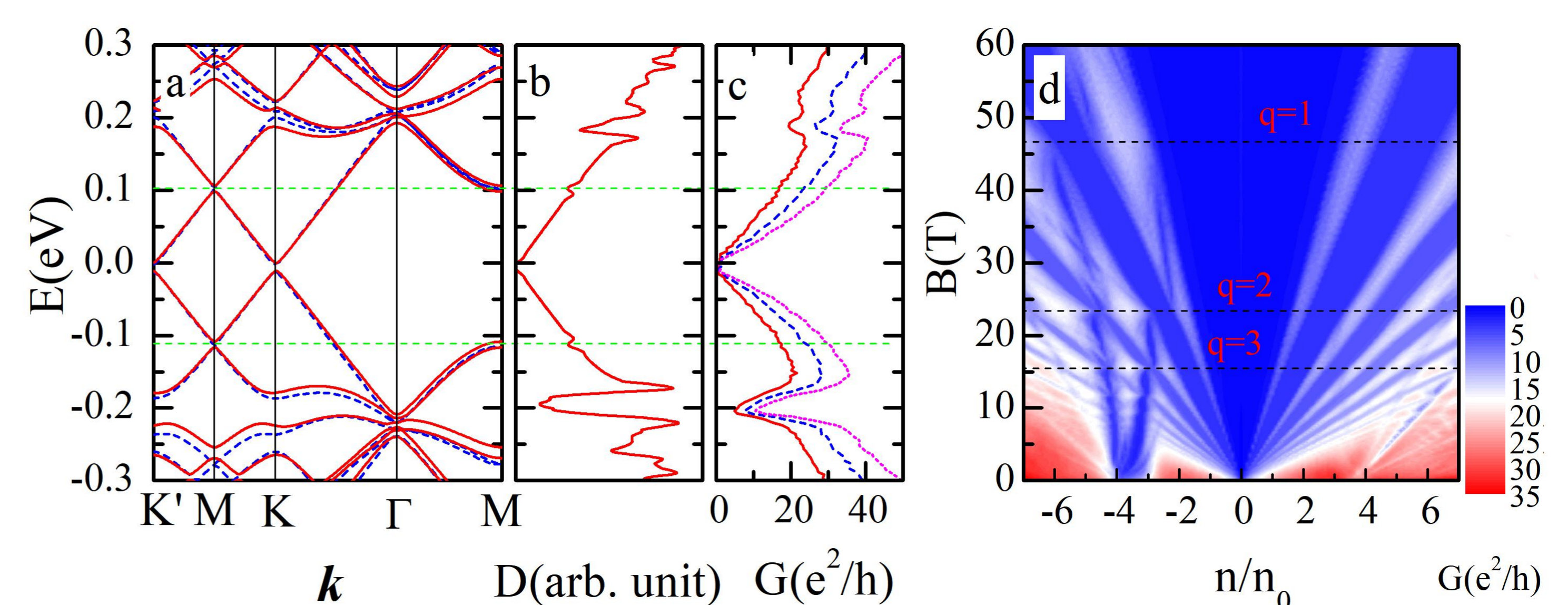
### Electronic structure



**a., b., and c.** are calculated band structures; **d., e., and f.** are density of states; **g., h., and i.** are conductance with zero magnetic field. In the band structure and DOS, the red dashed lines denote the graphene monolayer for comparison. Here, **a., d., g.** are for twist angle  $0.0^\circ$ , **b., e., h.** are for twist angle  $0.5032^\circ$ , and **c., f., and i.** are for twist angle  $1.0047^\circ$ .

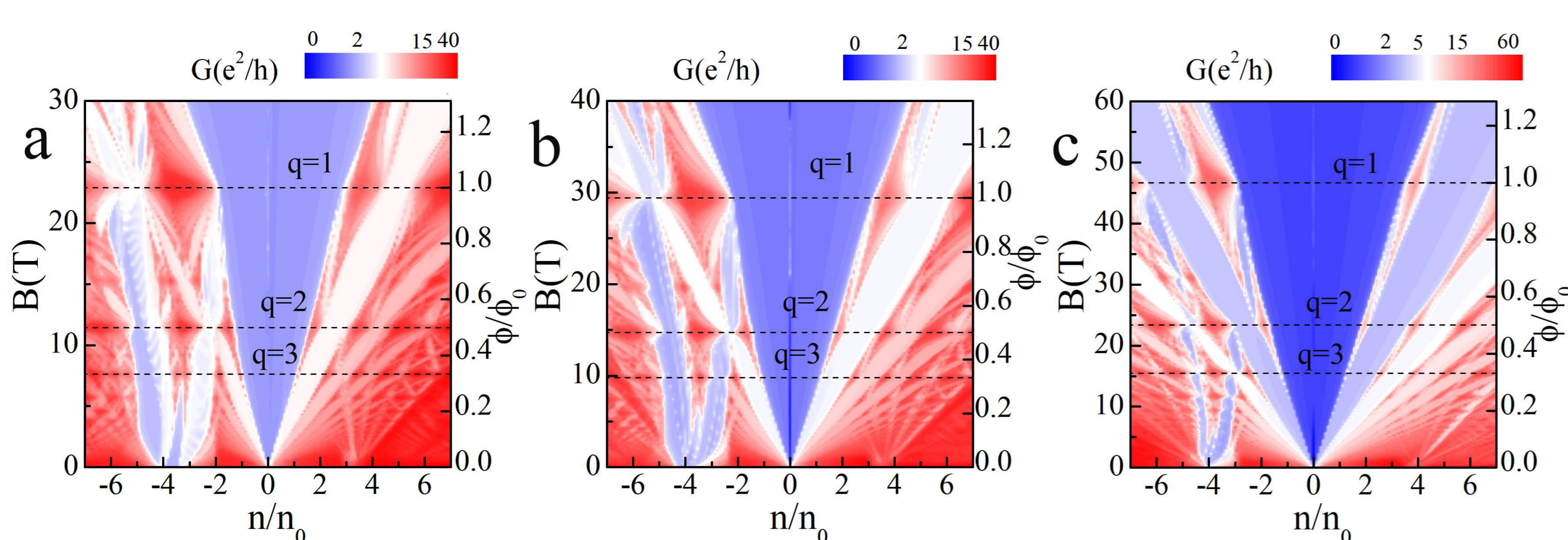
In the conductance (g,h,i) the red solid, blue dashed, and magenta dot lines are calculated for device sizes  $200\text{ nm} \times 200\text{ nm}$ ,  $300\text{ nm} \times 300\text{ nm}$ , and  $400\text{ nm} \times 400\text{ nm}$ , respectively.

### Disorder



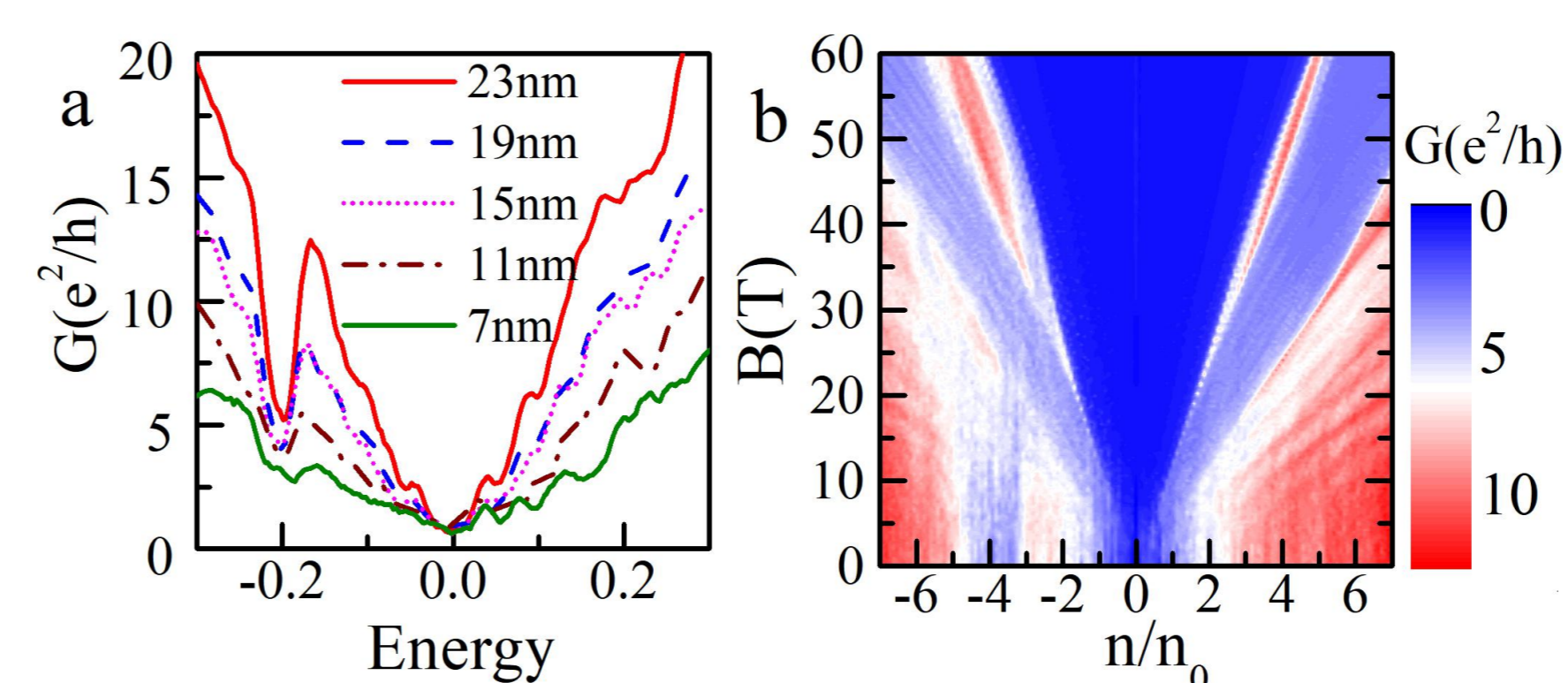
The electronic structure and conductance of G/hBN with disorder with twist angle  $1.0047^\circ$ . **a.** Red solid line: band structure with disorder. Dashed blue line: band structure for pristine sample. **b.** Density of states. **c.** Zero-field conductance. Red, blue, and magenta lines refer to device sizes of  $200\text{ nm} \times 200\text{ nm}$ ,  $300\text{ nm} \times 300\text{ nm}$  and  $400\text{ nm} \times 400\text{ nm}$ , respectively. **d.** Magnetoconductance for a disordered sample.

### Magnetotransport



Longitudinal magnetoconductance  $G$  as a function of magnetic field and electron density.  $n$  is electron density, and  $n_0$  is the electron density per each Bloch band. Right vertical axis is scaled by  $\phi/\phi_0$  where  $\phi$  is the flux through one moiré unit cell and  $\phi_0 = h/e$  is the flux quantum. Dashed black lines show  $q=1, 2$ , and  $3$ , where the Landau levels intersect. **a., b., and c.** are for twist angle =  $0.0^\circ$ ,  $0.5032^\circ$ , and  $1.0047^\circ$ , respectively.

### Antidot lattice



**a.** Conductance for antidot lattices with varying neck lengths  $d_N$ . For neck length  $d_N$  smaller than the moiré length  $\lambda$  ( $10.1\text{ nm}$ ), the secondary feature vanishes. **b.** Landau fan diagram with antidot lattice ( $d_N=15\text{ nm}$ ).

### Conclusion

The calculated electronic structure and transport are in excellent agreement with experimental data. Although disorder can lift the degeneracy of the bands at high symmetry points, the main features of band are similar to the clean case while the magnetoconductance stays unchanged. The electronic and transport behavior of G/hBN with antidot lattice reveals that the secondary Dirac point will disappear once the neck width  $d_N$  is smaller than the moiré wave length  $\lambda$ .

### References

1. L. Banszerus, *et al.* Sci. Adv. 1, e1500222 (2015).
2. B. S. Jessen, *et al.* Nat. Nanotechnol. 14, 1029-1034 (2019).
3. C. R. Dean, *et al.* Nature 497, 598-602 (2013).
4. B. Hunt, *et al.* Science 340, 1427-1431 (2013).

Corresponding author:  
yongdu@dtu.dk